Polarization converters in highly birefringent microfibers

HaiFeng Xuan,[1,2] **Jun Ma,**[1] **Wa Jin,**[1] **and Wei Jin**[1,2,*]

[1]*Department of Electrical Engineering, The Hong Kong Polytechnic University, Hong Kong*

[2]*The Hong Kong Polytechnic University Shenzhen Research Institute, Shenzhen, China*

[*]*eewjin@polyu.edu.hk*

Abstract: A novel type of polarization converters (PCs) based on highly birefringent (Hi-Bi) microfibers is presented. Analytical formulation based on the Jones Matrix method and a numerical code based on the Full Vectorial Finite Difference Beam Propagation Method are developed to analyze the polarization evolutions in such PCs. Two different design configurations, namely the "one-side" and "two-side" perturbation configurations, are studied by use of the two methods, and the results obtained agree well with each others. The PCs can be flexibly designed to have different operating wavelengths, spectral bandwidths, and devices lengths. A particular PC based on an elliptical microfiber demonstrates a bandwidth of $\sim$ 600 nm around 1550 nm with a device length of $\sim$ 150 μm.

OCIS codes: (060.2420) Fibers, polarization-maintaining; (060.2340) Fiber optics components; (060.4005) Microstructured fibers; (230.5440) Polarization-selective devices.

References and links

1. L. Tong, R. R. Gattass, J. B. Ashcom, S. He, J. Lou, M. Shen, I. Maxwell, and E. Mazur, "Subwavelength-diameter silica wires for low-loss optical wave guiding," Nature **426**, 816–819 (2003).
2. L. Tong, J. Lou, R. R. Gattass, S. He, X. Chen, Liu, and E. Mazur, "Assembly of silica nanowires on silica aerogels for microphotonic devices," Nano Lett. **5**, 259–262 (2005).
3. G. Brambilla, V. Finazzi, and D. Richardson, "Ultra-low-loss optical fiber nanotapers," Opt. Express **12**, 2258–2263 (2004).
4. M. Sumetsky, "Basic elements for microfiber photonics: micro/nanofibers and microfiber coil resonators," J. Lightwave Technol. **26**, 21–27 (2008).
5. H. F. Xuan, W. Jin, and M. Zhang, "CO2 laser induced long period gratings in optical microfibers," Opt. Express **17**, 21882–21890 (2009).
6. H. F. Xuan, W. Jin, and S. Liu, "Long-period gratings in wavelength-scale microfibers," Opt. Lett. **35**, 85–87 (2010).
7. X. Fang, C. R. Liao, and D. N. Wang, "Femtosecond laser fabricated fiber Bragg grating in microfiber for refractive index sensing," Opt. Lett. **35**, 1007–1009 (2010).
8. J. L. Kou, S. J. Qiu, F. Xu, and Y. Q. Lu, "Demonstration of a compact temperature sensor based on first-order bragg grating in a tapered fiber probe," Opt. Express **19**, 18452–18457 (2011).
9. H. F. Xuan, J. Ju, and W. Jin, "Highly birefringent optical microfibers," Opt. Express **18**, 3828–3839 (2010).
10. J. Noda, K. Okamoto, and Y. Sasaki, "Polarization-maintaining fibers and their applications," J. Lightwave Technol. **4**, 1071–1089 (1986).
11. R. Bergh, H. Lefevre, and H. J. Shaw, "An overview of fiber-optic gyroscopes," J. Lightwave Technol. **2**, 91–107 (1984).
12. Y. Shani, R. Alferness, T. Koch, U. Koren, M. Oron, B. I. Miller, and M. G. Young, "Polarization rotation in asymmetric periodic loaded rib waveguides," Appl. Phys. Lett. **59**, 1278–1280 (1991).
13. G. Statkiewicz-Barabach, A. Anuszkiewicz, W. Urbanczyk, and J. Wojcik, "Sensing characteristics of rocking filter fabricated in microstructured birefringent fiber using fusion arc splicer," Opt. Express **16**, 17258–17268 (2008).

#195146 - $15.00 USD Received 5 Aug 2013; revised 29 Nov 2013; accepted 30 Nov 2013; published 7 Feb 2014

14. T. Mangeat, L. Escoubas, F. Flory, L. Roussel, M. De Micheli, and P. Coudray, "Integrated polarization rotator made of periodic asymmetric buried Ta2O5 / silica sol-gel waveguides," Opt. Express **15**, 12436–12442 (2007).
15. K. Bayat, S. K. Chaudhuri, and S. Safavi-Naeini, "Ultra-compact photonic crystal based polarization rotator," Opt. Express **17**, 7145–7158 (2009).
16. R. H. Stolen, A. Ashkin, W. Pleibel, and J. M. Dziedzic, "In-line fiber-polarization-rocking rotator and filter," Opt. Lett. **9**, 300–302 (1984).
17. R. Kaul, "Pressure sensitivity of rocking filters fabricated in an elliptical-core optical fiber," Opt. Lett. **20**, 1000 (1995).
18. G. Kakarantzas, A. Ortigosa-Blanch, T. a. Birks, P. S. J. Russell, L. Farr, F. Couny, and B. J. Mangan, "Structural rocking filters in highly birefringent photonic crystal fiber," Opt. Lett. **28**, 158–160 (2003).
19. W. P. Huang, M. Z. Mao, "Polarization rotation in periodic loaded rib waveguides," J. Lightwave Technol. **10**, 1825–1831 (1992).
20. S. Obayya, B. Rahman, and H. El-Mikati, "Vector beam propagation analysis of polarization conversion in periodically loaded waveguides," IEEE Photonics Technol. Lett. **12**, 1346–1348 (2000).
21. R. Scarmozzino, A. Gopinath, R. Pregla, and S. Helfert, "Numerical techniques for modeling guided-wave photonic devices," IEEE J. Sel. Top. Quantum Electron. **6**, 150–162 (2000).
22. J. Broeng, S. E. Barkou, T. Søndergaard, and A. Bjarklev, "Analysis of air-guiding photonic bandgap fibers," Opt. Lett. **25**, 96–98 (2000).
23. W. P. Huang and C. L. Xu, "Simulation of three-dimensional optical waveguides by a full-vector beam propagation method," J. Lightwave Technol. **29**, 2639–2649 (1993).
24. J. Yamauchi, G. Takahashi, and H. Nakano, "Full-vectorial beam-propagation method based on the McKee-Mitchell scheme with improved finite-difference formulas," J. Lightwave Technol. **16**, 2458–2464 (1998).
25. F. Fogli, L. Saccomandi, P. Bassi, G. Bellanca, and S. Trillo, "Full vectorial BPM modeling of index-guiding photonic crystal fibers and couplers," Opt. Express **10**, 54–59 (2002).
26. G. R. Hadley, "Transparent boundary condition for beam propagation," Opt. Lett. **16**, 624–626 (1991).
27. J. Shibayama, M. Sekiguchi, J. Yamauchi, and H. Nakano, "Eigenmode analysis of optical waveguides by an improved finite-difference imaginary-distance beam propagation method," Electron. Comm. Jpn. 2 **81**, 1–9 (1998).
28. I. Giuntoni, D. Stolarek, H. Richter, S. Marschmeyer, J. Bauer, A. Gajda, J. Bruns, B. Tillack, K. Petermann, and L. Zimmermann,"Deep-UV technology for the fabrication of Bragg gratings on SOI rib waveguides," IEEE Photonics Technol. Lett. **21**, 1894–1896 (2009).

1. Introduction

Recently, there has been considerable interest in micro/nanofiber (MNF) based photonic devices, circuits and applications. Optical MNFs can be taper-drawn from standard optical fibers or glass rods and have potential to be used as low-loss micro/nano scale optical waveguides [1–4]. So far most research exploits the strong external evanescent fields associated with MNFs, though there are also reports on MNF based mode-coupling devices such as long period gratings (LPGs) [5, 6] and fiber Bragg gratings (FBGs) [7, 8]. Recently, highly birefringent (Hi-Bi) MNFs have been fabricated and it demonstrates capability of maintaining the state of polarization during light transmission [9]. These MNFs would find applications in MNF-based interferometric sensors and coherent transmission systems [10, 11].

Polarization converters (PCs) refer to a class of devices that convert a polarization eigenmode in a polarization maintaining Hi-Bi waveguide to orthogonal polarization eigenmode. They are essential functional components in guided wave optical systems such as polarization diversity heterodyne receivers and highly sensitive fiber sensors [12, 13]. PCs have been implemented in rib [12], buried [14] and photonic crystal [15] waveguides, and they are very compact in size but difficult to be integrated into optical fiber systems because of the large fiber-waveguide coupling loss [12]. PCs based on conventional [16, 17] and photonic crystal [18] Hi-Bi fibers have been reported, these devices have a length of a few centimeters and can be conveniently integrated into standard-size optical fiber systems.

In this paper, we present a novel class of Hi-Bi microfiber PCs and report the results of our theoretical and numerical investigation of such PCs. The microfiber PCs are fabricated directly on fiber-tapers made from standard-size optical fibers and hence can easily be integrated into optical fiber systems with low loss. In addition, the microfiber PCs are flexible and have a device length of a few hundreds of micrometers, which might be used in future MNF-based integrated

#195146 - $15.00 USD Received 5 Aug 2013; revised 29 Nov 2013; accepted 30 Nov 2013; published 7 Feb 2014

optical circuits [1, 2]. Two PC configurations are proposed, and their polarization-converting and spectral properties are studied by use of a self-developed code based on the Full Vectorial Finite Difference Beam Propagation Method (FV-FDBPM).

2. Analysis of Hi-Bi microfiber by FV-FDBPM

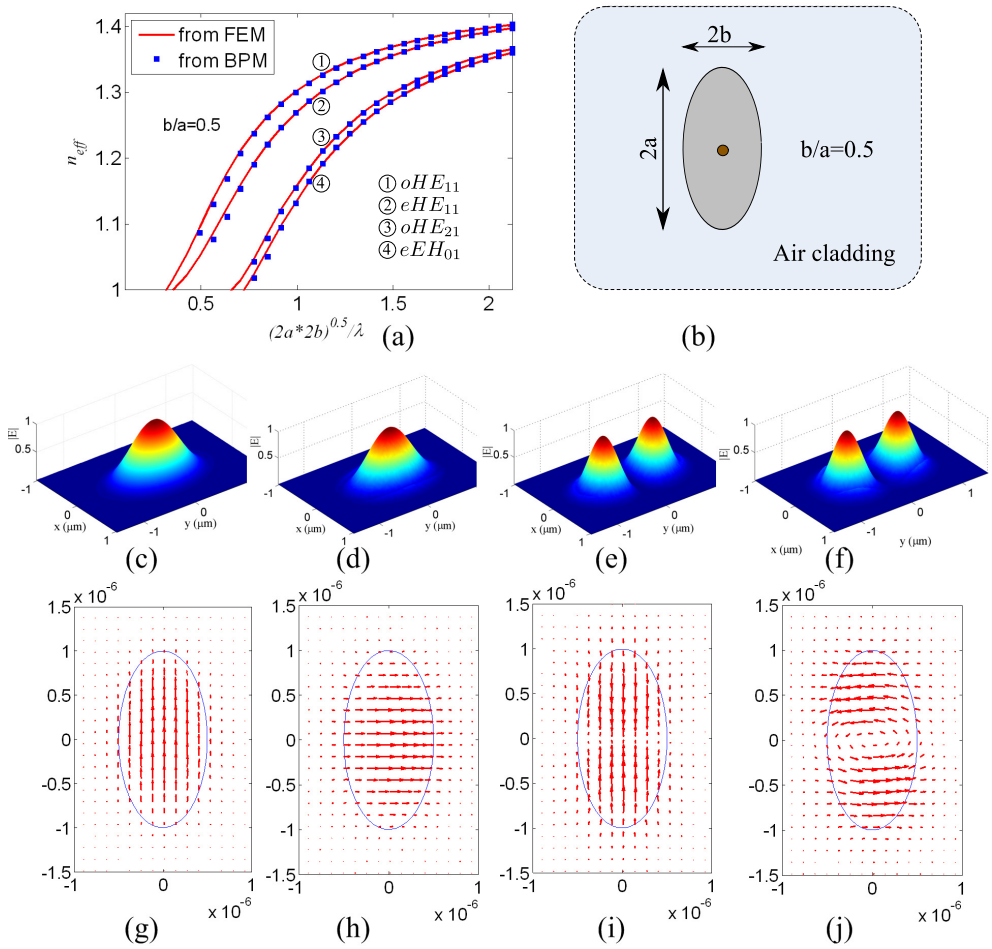

Fig. 1. Modal properties of an elliptical Hi-Bi microfiber calculated by use of the FV-FDBPM code and the FEM software. (a) Dispersion curves of the four lowest-order modes for $b/a = 0.5$; (b) The three-region model of the air-clad Hi-Bi microfiber. This model has been used to model a practical Hi-Bi microfiber fabricated previously [9]. (c)–(f) mode intensity distributions and (g)–(j) field vectors of the four modes. (c) and (g): oHE$_{11}$ mode; (d) and (h): eHE$_{11}$ mode; (e) and (i): oHE$_{21}$ mode; (f) and (j): eEH$_{01}$ mode.

Beam Propagation Method (BPM) is an effective method for studying wave propagation in waveguides and has been successfully employed to model polarization evolutions in various waveguides [19–21]. Since MNFs have a high core-cladding refractive-index contrast and their fields have significant vectorial characteristics [22], we here apply the full vectorial version of BPM [23–25] to study the MNF-based PCs. We implemented a three-dimension FV-FDBPM code based on the McKee-Mitchell alternating-direction implicit (ADI) method, the Douglas-

#195146 - $15.00 USD Received 5 Aug 2013; revised 29 Nov 2013; accepted 30 Nov 2013; published 7 Feb 2014

Rachford splitting [23, 24] and the Transparent Boundary Condition (TBC) [26]. Our FV-FDBPM code is firstly validated by applying it to calculate the modal and dispersion properties of an air-cladding Hi-Bi microfiber and comparing with the results obtained previously from a Full Vector Finite Element Method (FV-FEM) [9].

The model used to study the properties of the air-cladding Hi-Bi microfiber is shown in the Fig. 1(b). It comprises an infinite air-cladding and an elliptical core made predominantly of silica with a tiny circular Ge-doped center region. The Hi-Bi microfiber is featured with a semi-major diameter "a" and a semi-minor diameter "b", which are taken to be $a = 1$ μm and $b = 0.5$ μm, respectively. The refractive indices of the air-cladding, the silica and Ge-doped regions are set, respectively, to n_{air} = 1 , n_{silica} = 1.444 , and n_{Ge} = (1 + 0.36%) n_{silica}. The FV-FDBPM computational transverse domain is $5a \times 4b$ and a grid of 195×80 is used as the mesh for the finite-difference computation. The transverse grid constant is $dx = dy = 0.026$ μm, while the longitudinal interval between sampling points is $dz = 5dx$.

Figure 1 shows the calculated dispersion and field distribution characteristics of the four lowest-order modes. The results were obtained from the eigenmodes calculation in which the Imaginary Distance Propagating method [27] was incorporated into the FV-FDBPM code to speed up convergence. The first two modes are the oHE$_{11}$and eHE$_{11}$, while the second order modes are oHE$_{21}$ and eEH$_{01}$ modes. These four modes correspond, respectively, to the degenerated fundamental modes (HE$^x_{11}$, HE$^y_{11}$) and the second order modes (HE$_{21}$, TE$_{01}$) in a circular air-cladding microfiber. However, they are no longer degenerate in the Hi-Bi microfiber.

The power distributions of the four modes are shown in Figs. 1(c)–1(f) while the electric field vectors are in Figs. 1(g)–1(j). As shown in the Fig. 1(a), the modal dispersions calculated by the FV-FDBPM (marked as solid points) and by the FV-FEM (marked as lines) are in good agreement with each other.

3. Design and analysis of polarization converters

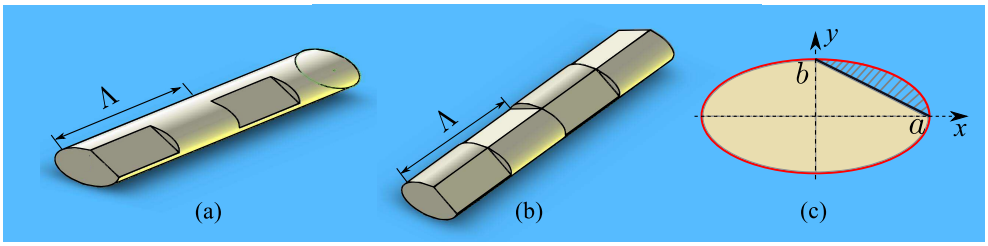

Fig. 2. Two configurations of Hi-Bi microfiber-based PCs: (a) Fiber surface perturbed from "one-side", (b) Fiber surface perturbed from "two-sides", (c) the cross-section of a perturbed region.

It's been known that asymmetric perturbation of a waveguide causes coupling between two orthogonal polarization modes and periodic application of such perturbations allow coherent accumulation of the coupled polarization mode [12, 14, 16, 18]. Figures 2(a) and 2(b) show two possible designs to achieve polarization coupling or conversion in an elliptical microfiber. In the first configuration, the microfiber is perturbed periodically on the same side of the ellipse as shown in Figs. 2(a) and 2(c); while in the second configuration, the cross-section is perturbed alternatively from two different sides of the ellipse, as shown in Fig. 2(b). The pitch or period (Λ) of the perturbation is chosen to satisfy the phase matching condition [12, 14]

$$\Lambda = \frac{\lambda}{\Delta n_{eff}} \tag{1}$$

#195146 - $15.00 USD Received 5 Aug 2013; revised 29 Nov 2013; accepted 30 Nov 2013; published 7 Feb 2014

where λ is the light wavelength in vacuum and Δn_{eff} is the difference in the effective indices of the oHE$_{11}$ and eHE$_{11}$ modes. Both structures in Fig. 2 might be fabricated by focused ion beam (FIB) milling [8], lithography-etching [12], Deep-UV lithography technologies [28], or a precision femtosecond laser micromachining system [6].

3.1. *Enhancement of non-dominant electric field*

The vector fields of the fundamental oHE$_{11}$ and eHE$_{11}$ modes are dominated respectively by the field components with polarization directions along the major- and minor-axes of the ellipse. With the coordinate system (x,y) in Fig. 2(c), the non-dominant field component of eigenmode oHE$_{11}$ in a perfect elliptical fiber is oHE$^y_{11}$, which is typically much smaller than the dominant field component oHE$^x_{11}$. Similarly, the non-dominant field component of orthogonal eigenmode (i.e., eHE$_{11}$) is eHE$^x_{11}$ and is also much smaller than dominant field component eHE$^y_{11}$.

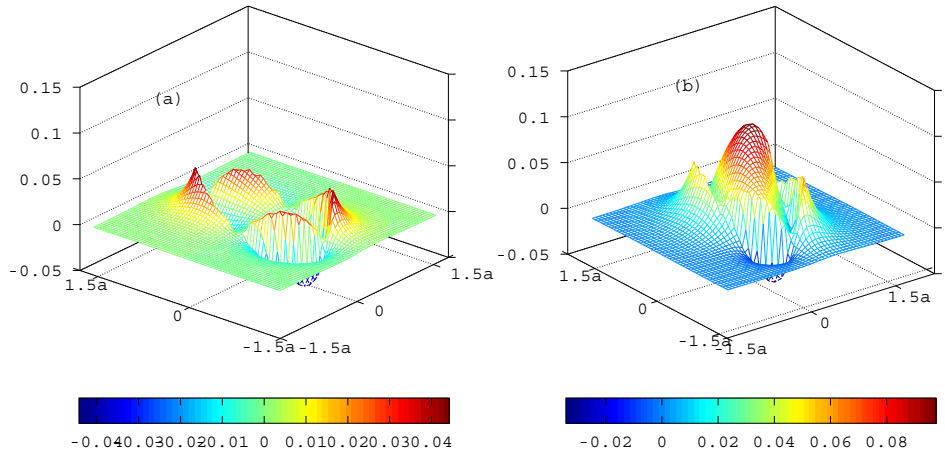

Fig. 3. 3D view of field components (oHE$^y_{11}$) of the eigenmode oHE$_{11}$ in (a) a perfect elliptical microfiber and (b) a perturbed elliptical microfiber. The cross-section of the perturbed microfiber is shown in Fig. 2(c) and b/a=0.5.

By introducing an asymmetric perturbation, the symmetry of the ellipse is altered and the local fields are tilted and subsequently the hybrid nature of the modes is enhanced. Figures 3(a) and 3(b) show the calculated electric field component (oHE$^y_{11}$) of the oHE$_{11}$ mode for a perfect elliptical Hi-Bi microfiber in Fig. 2 and the same fiber with a perturbation. The parameters of the elliptical microfiber are $a = 0.8$ μm and $b = 0.5a$, and perturbation is to remove the shaded region as shown in Fig. 2(c). The shaded region is bounded by a minor elliptic arc and a straight line connecting the arc's endpoints. Obviously, the field components (oHE$^y_{11}$) are dramatically enhanced near the flat facet. In Fig. 3, the field components oHE$^y_{11}$ are normalized by local field components oHE$^x_{11}$.

To view more clearly the enhancement of the field component oHE$^y_{11}$, the contours of field components oHE$^y_{11}$ as well as the electric field vectors of oHE$_{11}$ modes for the perfect and the perturbed structures are shown in the Figs. 4(a) and 4(b), respectively. The contours of electrical field components oHE$^x_{11}$ are not shown, since they are close to a Gaussian distribution and well known. As can be seen from Fig. 4, the field components oHE$^y_{11}$ in the perturbed structure is significantly enhanced as compared with the unperturbed structure; this would increase the overlap with the field component eHE$^y_{11}$ of eHE$_{11}$ and cause efficient coupling between the two polarization modes. This is the physical basis of the PC to be described in the following

#195146 - $15.00 USD Received 5 Aug 2013; revised 29 Nov 2013; accepted 30 Nov 2013; published 7 Feb 2014

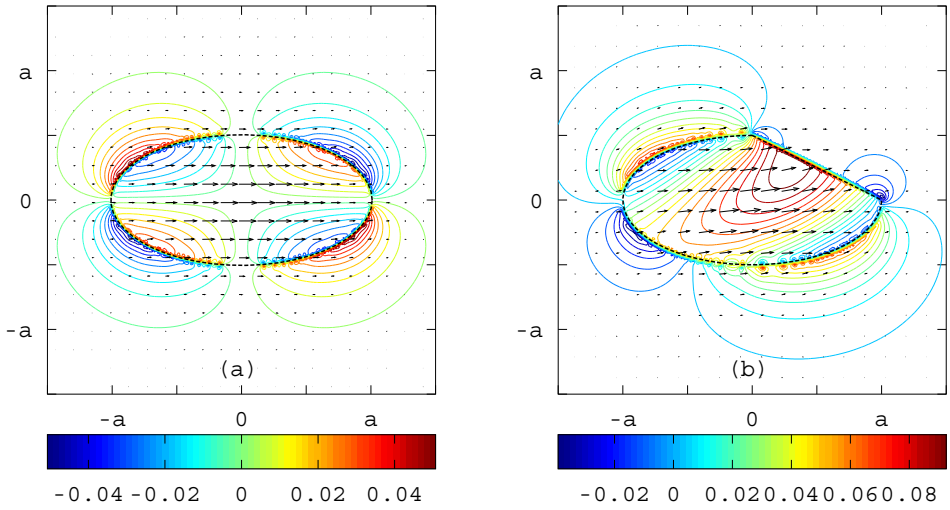

Fig. 4. Contour plotting of the field components ($o\mathrm{HE}_{11}^{y}$) and the electric field vectors of the fundamental $o\mathrm{HE}_{11}$ mode in the perfect (a) and the perturbed microfiber (b).

sections.

To investigate the effect of varying geometry of perturbation on the polarization mode coupling, we define a normalized overlap integral between orthogonal polarization modes as follows

$$\alpha = \frac{< o\mathbf{HE}_{11}, e\mathbf{HE}_{11} >}{|o\mathbf{HE}_{11}| \cdot |e\mathbf{HE}_{11}|} = \frac{\left| \int_{\Omega} o\mathrm{HE}_{11}^{y} \cdot e\mathrm{HE}_{11}^{y} \mathrm{d}_{\Omega} + \int_{\Omega} o\mathrm{HE}_{11}^{x} \cdot e\mathrm{HE}_{11}^{x} \mathrm{d}_{\Omega} \right|}{\left| \int_{\Omega} o\mathrm{HE}_{11} \cdot o\mathrm{HE}_{11}^{*} \mathrm{d}_{\Omega} \cdot \int_{\Omega} e\mathrm{HE}_{11} \cdot e\mathrm{HE}_{11}^{*} \mathrm{d}_{\Omega} \right|^{0.5}} \tag{2}$$

It should be mentioned that two fields ($o\mathbf{HE}_{11}$and $e\mathbf{HE}_{11}$) used in the integration are not from the same longitudinal location, but instead from adjacent half-period subsections. A larger value of parameter α would mean stronger coupling between the two polarization modes or better polarization converting efficiency.

We numerically calculated the values of α for various different perturbation geometries shown in Figs. 5(a) and 5(c), and the results are presented in Figs. 5(b) and 5(d). Figure 5(a) shows a serial of nine different perturbation geometries, achieved by "cutting" away part of the ellipse along a straight line with different azimuth angles (θ) from 0.15π to 0.85π. For the purpose of comparison, the "cutting away" areas for all the nine geometries are the same and equal to the shaded which are defined by the straight line $y = -b/a(x-a)$ and the minor arc of the ellipse. The value of α calculated form Eq. (2) raises from ~ 0.01 for an azimuth angle of $\theta = 0.15\pi$ to a maximum value of ~ 0.084 for $\theta = 0.5\pi$, and reduces to ~ 0.01 when θ is further increased to 0.85π. This shows that the highest polarization converting efficiency is achieved for $\theta = 0.5\pi$, corresponding to a "cutting away" along the line $y = -b/a(x-a)$.

For the same azimuth angle of $\theta = 0.5\pi$, the effect of cutting away depth is also studied and shown in the Figs. 5(c) and 5(d). The straight lines in Fig. 5(c) is described by $y = -b/a(x-a) + \delta$, where δ referred as the "depth" of the cutting away. As shown in Fig. 5(d), α increases with the decreasing δ (deeper cut), and a too shallow cut (with bigger δ) would lead to ineffective polarization converting, while a too deep cut would caused a large

#195146 - $15.00 USD Received 5 Aug 2013; revised 29 Nov 2013; accepted 30 Nov 2013; published 7 Feb 2014

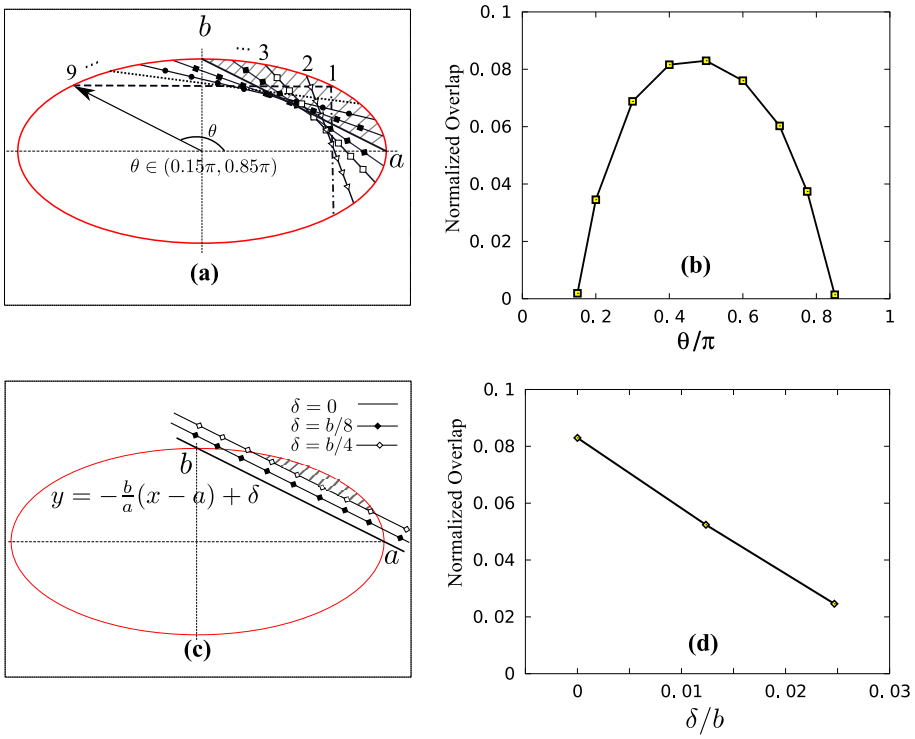

Fig. 5. The value of parameter α for different perturbation geometries. (a) Different azimuth angle θ and (b) corresponding value of α ; (c) Different depth δ and (d) corresponding value of α .

device loss.

3.2. *Analytical formulation*

The asymmetric perturbation of the elliptical fiber produces a tilt of its local electrical field and the principal birefringence axes of the perturbed region may then be regarded being rotated by angle γ, which may be evaluated by

$$\gamma = \pi/2 - \arccos(\alpha) \tag{3}$$

where α is defined in Eq. (2). Figures 6(a) and 6(b) show the cross-sectional profiles of the fiber and the corresponding principal axes at different waveguide subsections. For the configuration shown in Fig. 6(a), the principal axes of the perturbed region (i.e., V_s^- and V_f^-) differ from the original axes of the elliptical fiber (i.e., x and y) by an angle γ, while for the design in Fig. 6(b) the rotation between principal axes of the two subsequent sections (i.e. from V_s^-, V_f^- to V_s^+, V_f^+) is 2γ. The angle of rotation within one period of perturbation is shown schematically in the Figs. 6(c) and 6(d), and angle of rotation may be expressed as

$$\psi = n\gamma,\ n = 1\ or\ 2 \tag{4}$$

with n = 1 for the design in Figs. 6(a) and 6(c), and n = 2 in Figs. 6(b) and 6(d).

Based on the above understanding, we may use the Jones Matrix Method (JMM) to model the polarization evaluation of the PCs. It has been shown that the JMM is as effective as the Coupled Mode Method in analyzing polarization rotation devices [19] but gives a clearer physical

#195146 - $15.00 USD Received 5 Aug 2013; revised 29 Nov 2013; accepted 30 Nov 2013; published 7 Feb 2014

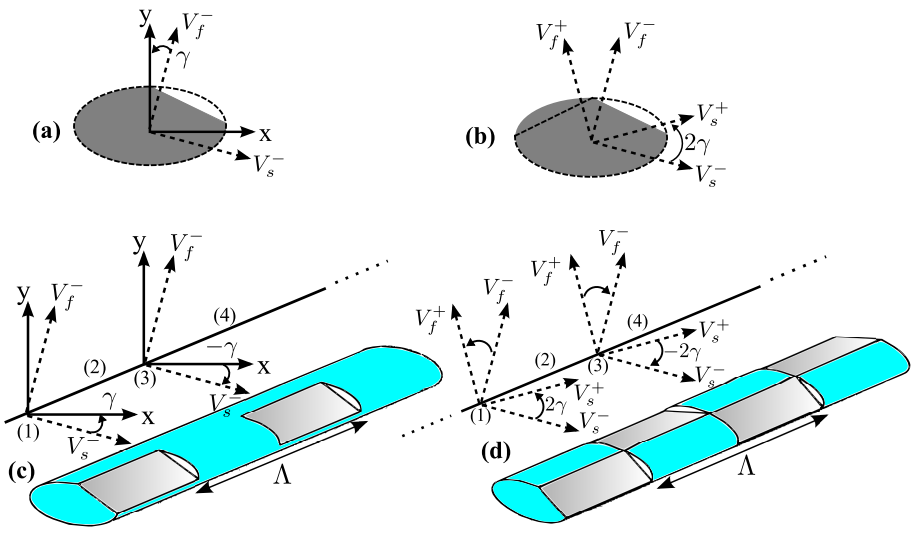

Fig. 6. Schematics demonstrating the different waveguide geometries and birefringent principal axes. Elliptical microfiber with one-side ((a) and (c)) and two-side ((b) and (d)) perturbations. (x,y) coordinates are aligned to the principal axes of the original elliptical microfiber, they are defined in Fig. 2(c) ; (V_s^-, V_f^-) and (V_s^+, V_f^+) are the principal axes of the perturbed sections, and they can be obtained respectively by rotating (x,y) clockwise and anti-clockwise by an angle γ.

picture. To model polarization evolution in Hi-Bi microfiber PCs, the polarized light needs to be decomposed locally into a linear combination of the "fast" and "slow" polarization modes and, at the interface of adjacent subsections, transformation between different coordinate systems need to be implemented.

Assume that the incident beam is described by the Jones Vector $V_{in} = \begin{bmatrix} V_x \\ V_y \end{bmatrix}$, where V_x and V_y are two complex components. For the "one-side" configuration shown in Fig. 6(c), the output polarization state $V_{out} = \begin{bmatrix} V_x' \\ V_y' \end{bmatrix}$ may be formulated by

$$\begin{bmatrix} V_x' \\ V_y' \end{bmatrix} = W_d^L R(-\psi) W_d^R R(\psi) \cdots W_d^L R(-\psi) W_d^R R(\psi) \begin{bmatrix} V_x \\ V_y \end{bmatrix} \tag{5}$$

$$R(\psi) = \begin{bmatrix} \cos\psi & \sin\psi \\ -\sin\psi & \cos\psi \end{bmatrix} \tag{6}$$

$$W_d^x = e^{-i\phi^x} \begin{bmatrix} \exp(-i\Gamma^x/2) & 0 \\ 0 & \exp(i\Gamma^x/2) \end{bmatrix} \tag{7}$$

where $R(\psi)$ is the coordinate transformation matrix at the waveguide interface and ψ is defined in Eq. (4); W_d^x is the Jones Matrix of the waveguide sections with $\Gamma^x = (\beta_s^x - \beta_f^x)\Lambda/2$ and $\phi^x = (\beta_s^x + \beta_f^x)\Lambda/4$. β_s^x and β_f^x are the propagation constants along the slow and fast axes respectively. $x = L$ or R represents the two subsections within a period Λ. For the "one-side" configuration considered here, R represents the perturbed half period while L represents the unperturbed half period. A similar formulation may be developed for the "two-side" configuration shown in Fig. 6(d).

The polarization evolution over one perturbation period may be described by the following product of matrices

#195146 - $15.00 USD Received 5 Aug 2013; revised 29 Nov 2013; accepted 30 Nov 2013; published 7 Feb 2014

$$W_\Lambda = W_d^L R(-\psi) W_d^R R(\psi) \tag{8}$$

Under the phase matching condition as defined in Eq. (1), Eq. (8) can be deduced as

$$W_\Lambda = \begin{bmatrix} -\cos 2\psi & -\sin 2\psi \\ \sin 2\psi & -\cos 2\psi \end{bmatrix} \tag{9}$$

Consider a simple case where only the x- polarized light (i.e, $o\mathrm{HE}_{11}$ mode in the Hi-Bi microfiber) is exited, then $V_{in} = \begin{bmatrix} 1 \\ 0 \end{bmatrix}$, the polarization state of the output light after propagating one period would be

$$\mathbf{V}' = \begin{bmatrix} -\cos 2\psi & -\sin 2\psi \\ \sin 2\psi & -\cos 2\psi \end{bmatrix} \begin{bmatrix} 1 \\ 0 \end{bmatrix} \equiv \begin{bmatrix} -\cos 2\psi \\ \sin 2\psi \end{bmatrix} \tag{10}$$

That is, the output polarization may be considered as linearly polarized but being rotated by a angle of 2ψ as compared with the input polarization. After propagating for N number of periods, the optical power of converted polarization mode (i.e., y-polarization) may be expressed as:

$$P = \sin^2(2\psi \cdot N) \tag{11}$$

where ψ should be taken as γ for the configuration in Fig. 6(c) and as 2γ for the configuration in Fig. 6(d). The maximum energy conversion between $o\mathrm{HE}_{11}$ and $e\mathrm{HE}_{11}$ modes occurs when the number of periods approximately satisfies

$$N_c = \pi/(4\psi) \tag{12}$$

and the device length can then be estimated to be $L_c = N_c \cdot \Lambda$.

In summary, in applying the above formulation, the field distributions in the two subsections within a period are firstly calculated, the values of ψ is then obtained by using Eqs. (2)–(4), and finally the polarization conversion efficiency and the number of periods required to achieve maximum polarization conversion are estimated by using Eqs. (11) and (12).

3.3. Numerical simulation and discussion

The analytical formulation in section 3.2 provides the "rule of the thumb" for the design of microfiber based PCs. In the following, we present the results of numerically simulation by use of the FV-FDBPM and compare with the results from the analytical formulation in Section 3.2. The elliptical microfiber studied has semi-diameters $a = 0.8\ \mu$m and $b = 0.5a$. The FV-FDBPM computational transverse domain is $4a \times 4a$ and the mesh grid used for finite-difference computation is 111×111. The transverse grid constant is $dx = dy = 0.0297\ \mu$m, while the spacing between the longitudinal sampling points is $dz = 3dx$.

Figure 7 shows the calculated evolutions of electric field distributions for the eigenmodes for a "two-side" configuration as shown in Fig. 6(d). The "cutting away" areas are defined by an azimuth angle of $\theta = \pi/2$ and a depth of $\delta = 0$. It is assumed that the x-polarization dominated eigenmode $o\mathrm{HE}_{11}$ is exited at the $z = 0$ and the pitch of the perturbation is 36 μm. It can be seen that the light power in the x-polarization is completely coupled to the y-polarization after a propagation distance of $\sim$ 144 μm or $\sim$ 4 periods. Light would couple back to the x-polarization after the maximum power transfer occur.

Figures 8(a) and 8(b) display the power exchanged between the two polarizations as the function of propagation distance for the "two-side" and "one-side" perturbation configurations respectively. The dotted lines are the raw results obtained from the FDBPM and it's obvious that the power losses increase with propagation distance, as can be seen from the Px(raw)

#195146 - $15.00 USD Received 5 Aug 2013; revised 29 Nov 2013; accepted 30 Nov 2013; published 7 Feb 2014

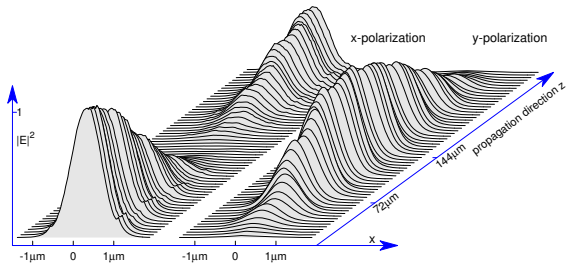

Fig. 7. Evolution of electric field distributions of two orthogonal polarizations in a microfiber-based PC.

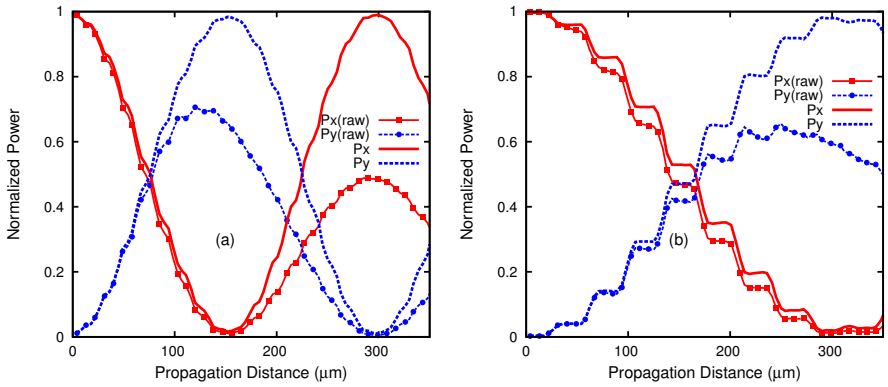

Fig. 8. Evolution of light power in two polarizations with propagation distance in microfiber-based PCs. (a) a "two-side" configuration, and (b) the "one-side" configuration.

and Py(raw) curves. The dash- and solid-lines are the normalized results which are calculated by using $P_i = P_i(raw)/[P_x(raw) + P_y(raw)]$, where i = x or y. It can be seen from Fig. 8 that number of period required for maximum conversion is ~ 4 for the two-side configuration and ~ 8 for the one-side configuration. This indicates that the converting efficiency of the double-side configuration is approximately twice that of the single-side configuration. This is consistent with the analytical formulation in Section 3.2 in which the polarization rotation angle ψ for the two-side configuration is twice that of the one-side configuration. This doubled device length of the one-side configuration could lead to narrower spectral bandwidth of the PCs, which will be discussed later in this section. From Fig. 8, the device losses corresponding to complete polarization conversions, which occurs at ~ 144 μm for the two-side configuration and ~ 288 μm for the one-side configuration, are ~ 1.9 dB and ~ 2.1 dB respectively. These values are similar to the PC fabricated on the rig waveguide [12]. The device loss is believed to arise mainly from the discontinuities between waveguide sections.

The polarization conversion characteristics of the microfiber PCs with different perturbation defined in Figs. 5(a) and 5(c) were studied by use of the FV-FDBPM code and the analytical formulation (the α-method), and the results for the two-side configuration are shown in Figs. 9 and 10. As shown in the Fig. 9(a), different θ leads to different propagating distance (L_c) for achieving total polarization conversion. The number of periods N_c required to achieve complete polarization conversion as function of azimuth angle is shown in the Fig. 9(b). The red square-

#195146 - $15.00 USD Received 5 Aug 2013; revised 29 Nov 2013; accepted 30 Nov 2013; published 7 Feb 2014

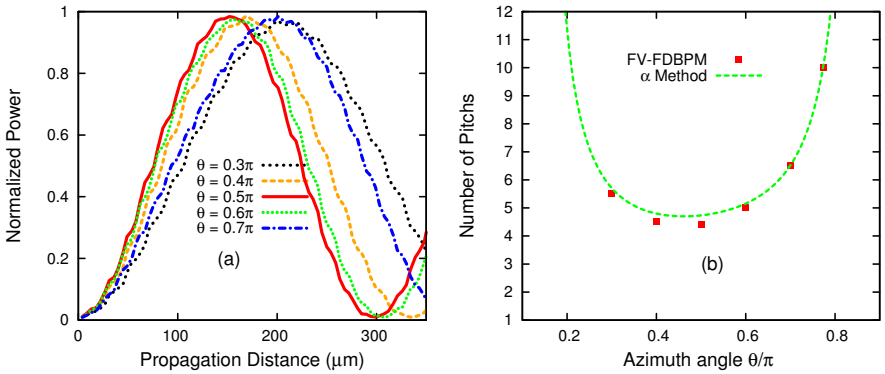

Fig. 9. Polarization evolutions for different perturbation azimuth angle θ (defined in Fig. 5(a)) (a) Normalized power of the coupled polarization as function of propagating distance for different θ values. (b) Number of periods needed to achieve complete polarization conversion for different θ values.

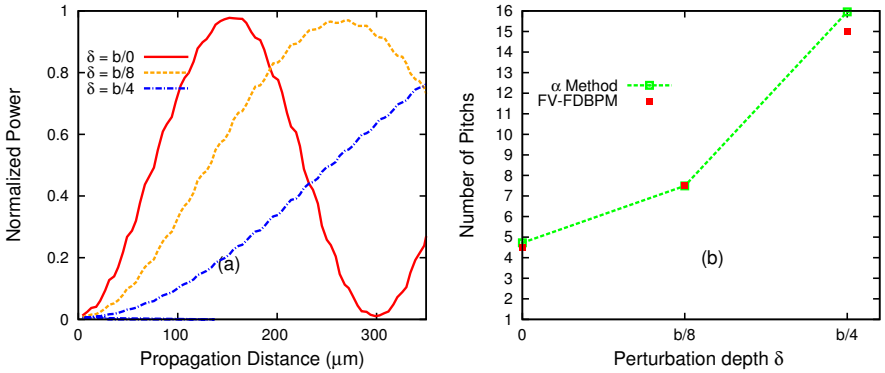

Fig. 10. Polarization evolutions for different perturbation depth δ (defined in Fig. 5(c)) in a Hi-bi microfiber PC with two-side deformations. (a) Normalized power of coupled polarization as function of propagation distance for different values of δ. (b) Number of periods needed to achieve complete polarization conversion as function of δ.

dots are the results from FV-FDBPM while the dashed line is from the analytical formulation described in Section 3.2. The close agreement between the two methods indicates the simple analytical formulation in Section 3.2 provides a good estimation for designing the microfiber-based PCs.

Likewise, Fig. 10 shows the polarization converting characteristics of PCs with different values of δ as defined in Fig. 5(c). The polarization converting efficiency decreases with increasing δ, and the the numbers of period N_c required for complete conversion increases with increasing value of δ. Again the results from the FV-FDBPM code and the α-method are congruous, which verifies the effectiveness of the analytical formulation in Section 3.2. The device loss for complete polarization conversion for δ = b/8 and from 0.3π to 0.6π are found to be less than 2.2 dB.

The functional spectral bandwidth of the presented Hi-Bi microfiber PCs is also investigated. As shown previously [9], the dispersion properties of the microfibers can be flexibly designed by varying the dimensions of the fibers, which may be exploited for designing microfiber PCs

#195146 - $15.00 USD Received 5 Aug 2013; revised 29 Nov 2013; accepted 30 Nov 2013; published 7 Feb 2014

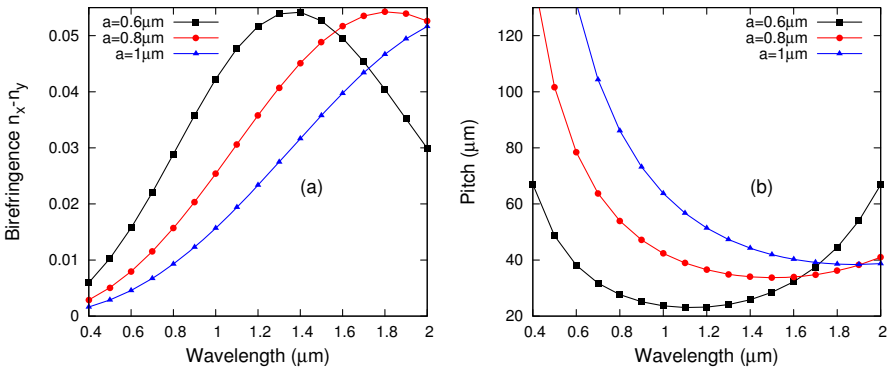

Fig. 11. (a) Birefringence as the functions of wavelength for various fiber semi-major diameters a ($b = 0.5a$); (b) pitches required for phase matching between the two polarizations as function of wavelength.

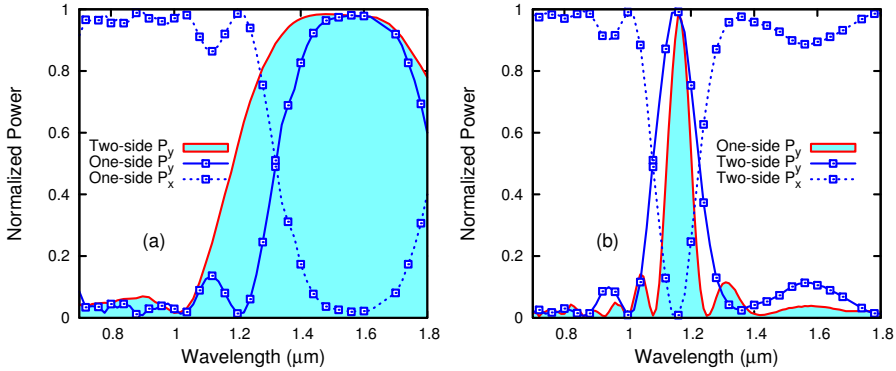

Fig. 12. Power exchange between two polarizations as the function of light wavelength. (a) $\Lambda = 36$ μm and only the coupled polarization (P_y) is shown for the two-side configuration. (b) $\Lambda = 42$ μm and only the coupled power is shown for the one-side configuration. The parameters of the Hi-Bi microfiber are same as in Fig. 8.

with different spectral bandwidth. As samples, Fig. 11(a) shows the birefringence of the fundamental modes as function of optical wavelength for elliptical microfibers with $b = 0.5a$ and $a = 0.5,\ 0.8\ ,1.0$ μm. The corresponding pitch to achieve phase matching or resonating coupling between the orthogonal polarizations as function of wavelength is shown in Fig. 11(b). The variation of birefringence and corresponding pitchs are dramatic for different values of semi-diameter a and these facts may be utilized to design PCs with different operating wavelengths and bandwidths. As shown in the Fig. 11(b), for different values of a, the "$\Lambda - \lambda$" curves have flat dispersion regions around different wavelength, and this property may be used to design broadband PCs at different wavelengths. Take the fiber with $a = 0.8$ μm as an example, the dispersion curve (the red circle-line in the Fig. 11(b)) exhibits a broad flat region around $\lambda = 1.5$ μm and $\Lambda = 35$ μm. This indicates that broadband PCs around 1.5 μm may be realized if the pitch of the PC is chosen to be ~ 35 μm. In addition, the very short device length (only 4 periods are required for the two-side configuration) which is resulted from the high polarization converting efficiency also leads to broadband performance. Thus, a combination of the flat phase matching curve and the short device length would allow PCs with a super

#195146 - $15.00 USD Received 5 Aug 2013; revised 29 Nov 2013; accepted 30 Nov 2013; published 7 Feb 2014

broad spectral bandwidth.

Figure 12 shows the power exchange between two polarizations as function of wavelength with different pitches for a Hi-Bi microfiber PC with $b = 0.5a$ and $a = 0.8$ μm. As shown in Fig. 12(a), the PC with the "two-side" configuration has $\sim$ 600 nm bandwidth. For the one-side configuration, shown as square-dotted lines, the conversion bandwidth is significantly narrower, indicating the effect of device length on the bandwidth of the PCs.

Figure 12(b) shows an example of PCs with a narrower converting bandwidth, obtained by operating at a higher slope point in the "$\Lambda - \lambda$" curve and using a longer device length. The setting of $\Lambda = 42$ μm leads to blue shift of the resonating wavelength to ~ 1.16 μm at which the dispersion slope is higher than at ~ 1.5 μm . The perturbation geometry used is shown in Fig. 5(c) with $\delta = b/8$, and this would result a weaker coupling and hence a longer propagating length to achieve maximum polarization conversion. The number of periods required for complete polarization conversion is N_c = 7 for the two-side configuration and N_c = 14 for the one-side configuration. The spectral bandwidth is obviously narrower for the one-side configuration because of the longer device length.

4. Conclusion

Novel PCs based on Hi-Bi microfibers are presented. The PCs may be made by periodically perturbing an elliptical microfiber asymmetrically from one side or two sides of the fiber surface. One possible fabrication method is to "cut" an elliptical fiber with a femtosecond infrared laser. A simplified analytical model based on the Jones Matrix formulation was developed to understand the physics behind the polarization conversion and to describe the process of polarization evolution when light propagate through different distance or number of perturbation periods. A self-developed FV-FDBPM code was used to simulate the details of polarization evaluations for different perturbation geometries characterized by the azimuth angle (θ) and depth (δ) of the perturbations. The device length, defined as the propagation distance where the power in one of polarizations is completely converted to orthogonal polarization, for the two-side configuration is about half of the one-side configuration for the same perturbation azimuth angle and depth. By varying the parameters of the elliptical fibers and the perturbation, the PCs may be flexibly designed to achieve different operating wavelengths, spectral bandwidths, and devices lengths. A particular PC based on an elliptical microfiber demonstrated a bandwidth of $\sim$ 600 nm around 1550 nm with a device length of only ~ 150 μm.

Acknowledgments

We acknowledge the support of Hong Kong SAR government through a GRF grant PolyU5177/10E, the National Natural Science Foundation of China through Grant No. 61290313, and the Hong Kong Polytechnic University through a postdoctoral fellowship grant.

#195146 - $15.00 USD Received 5 Aug 2013; revised 29 Nov 2013; accepted 30 Nov 2013; published 7 Feb 2014